Mon. Not. R. Astron. Soc. **000**, 000–000 (0000) Printed 23 February 2005 (MN LATEX style file v2.2)

An atlas of Calcium triplet spectra of active galaxies

A. Garcia-Rissmann[1⋆], L. R. Vega[1,2]†, N. V. Asari[1]‡, R. Cid Fernandes[1]§, H. Schmitt[3,4]¶, R. M. González Delgado[5]‖, T. Storchi-Bergmann[6⋆⋆]

[1] *Depto. de Física - CFM - Universidade Federal de Santa Catarina, C.P. 476, 88040-900, Florianópolis, SC, Brazil*
[2] *Observatorio Astronómico de Córdoba, Laprida 854, 5000, Córdoba, Argentina*
[3] *Remote Sensing Division, Code 7210, Naval Research Laboratory, 4555 Overlook Avenue, SW, Washington, DC 20375*
[4] *Interferometric Inc., 14120 Parke Long Court, 103, Chantilly, VA 20151*
[5] *Instituto de Astrofísica de Andalucía (CSIC), P.O. Box 3004, 18080 Granada, Spain*
[6] *Instituto de Física, Universidade Federal do Rio Grande do Sul, C.P. 15001, 91501-970, Porto Alegre, RS, Brazil*

23 February 2005

ABSTRACT

We present a spectroscopic atlas of active galactic nuclei covering the region around the $\lambda\lambda$8498, 8542, 8662 Calcium triplet (CaT). The sample comprises 78 objects, divided into 43 Seyfert 2s, 26 Seyfert 1s, 3 Starburst and 6 normal galaxies. The spectra pertain to the inner $\sim$ 300 pc in radius, and thus sample the central kinematics and stellar populations of active galaxies. The data are used to measure stellar velocity dispersions ($\sigma_\star$) both with cross-correlation and direct fitting methods. These measurements are found to be in good agreement with each-other and with those in previous studies for objects in common. The CaT equivalent width is also measured. We find average values and sample dispersions of $W_{\rm CaT}$ of 4.6 ± 2.0, $7.0\pm$ and 7.7 ± 1.0 Å for Seyfert 1s, Seyfert 2s and normal galaxies, respectively. We further present an atlas of [SIII]λ9069 emission line profiles for a subset of 40 galaxies. These data are analyzed in a companion paper which addresses the connection between stellar and Narrow Line Region kinematics, the behaviour of the CaT equivalent width as a function of $\sigma_\star$, activity type and stellar population properties.

Key words: galaxies: active - galaxies: Seyfert - galaxies: stellar content - galaxies: kinematics - galaxies: statistics

1 INTRODUCTION

Fifteen years ago, Terlevich, Díaz & Terlevich (1990, hereinafter TDT) carried out the first systematic study of the $\lambda\lambda$8498,8542,8662 Å absorption lines of the Ca II ion in active galactic nuclei (AGN). The main focus of that pioneer work on the "Calcium Triplet" (CaT) was on the equivalent width of this feature ($W_{\rm CaT}$), which provides both a stellar population diagnostic and a tool to investigate the presence of an underlying non-stellar continuum. Most of the AGN in the TDT sample were type 2 Seyferts. Their main finding was that $W_{\rm CaT}$ is remarkably similar for Seyfert 2s and normal galaxies, implying that the non-stellar featureless continuum (FC) invoked to account for the dilution of optical absorption lines in these objects either is not featureless at all or somehow disappears between optical and near-infrared (NIR) wavelengths. The interpretation advanced by TDT was that both the optical FC and the CaT lines are produced by a nuclear starburst. Subsequent work by the same group suggests that this may also apply to at least some type 1 Seyferts (Jiménez-Benito et al. 2000), although in the more active of these objects the AGN continuum does cause some dilution of the CaT.

Since then, the existence of starbursts around Seyfert 2 nuclei has been established by both indirect means (Cid Fernandes & Terlevich 1995; Heckman et al. 1995; Oliva et al. 1999) and direct detections of young stars by optical–UV imaging and spectroscopy (Heckman et al. 1997; González Delgado, Heckman & Leitherer 2001). While these studies confirmed that the optical FC of Seyfert 2s is predominantly due to recent star-formation, there are still doubts as to whether the CaT is produced by these starbursts or by older stars in the host galaxy bulge. In other words, it is not clear whether the CaT can be used to diagnose the presence of starbursts. Indeed, the mere fact that $W_{\rm CaT}$ shows

⋆ E-mail: aurea@astro.ufsc.br
† E-mail: luis@astro.ufsc.br
‡ E-mail: natalia@astro.ufsc.br
§ E-mail: cid@astro.ufsc.br
¶ E-mail: hschmitt@css.nrl.navy.mil
‖ E-mail: rosa@iaa.es
⋆⋆ thaisa@if.ufrgs.br

little variation among galaxies of widely different morphological and spectroscopic properties indicates that this feature may not be as simple a tracer of stellar populations as initially thought. Recent empirical and theoretical work reinforce this idea (Cenarro et al. 2003, 2004; Saglia et al. 2002; Falcón-Barroso et al. 2003; Michielsen et al. 2003; Thomas, Maraston & Bender 2003; Vazdekis et al. 2003), and show that there is still much to be learned about the CaT behaviour even in normal galaxies.

A more widespread use of the CaT nowadays is to measure stellar velocity dispersions ($\sigma_\star$). This was the approach followed by Nelson & Whittle (1995 and 1996; hereinafter collectively revered to as NW) in their comprehensive study of stellar and gaseous kinematics of AGN. The discovery of the relation between black-hole mass ($M_{\rm BH}$) and $\sigma_\star$ (Ferrarese & Merrit 2000; Gebhardt et al. 2000; Tremaine et al. 2002) brought renewed interest in this kind of work. Indeed, most of the current observational CaT studies in AGN are geared towards using this spectroscopic feature as an indirect black-hole weighing-scale (Ferrarese et al. 2001; Barth, Ho & Sargent 2002, 2003; Filippenko & Ho 2003; Barth et al. 2004; Botte et al. 2004; Nelson et al. 2004; Onken et al. 2004; Barth, Greene & Ho 2005). Finally, velocity dispersions are also useful to investigate stellar populations. Combined with size and luminosity measurements, $\sigma_\star$ allows the estimation of the mass-to-light ratio, which is a strong function of the age in stellar systems. There have been few applications of this idea to AGN, but the results reported so far seem to fit the scenario where active nuclei tend to be surrounded by stellar populations younger than those typical of elliptical galaxies and bulges (NW; Oliva et al. 1995; 1999).

This brief summary illustrates that there is plenty of motivation to study the CaT in both active and normal galaxies. In this paper we present an atlas of CaT spectra and related data products for a sample of 78 galaxies, most of which have active nuclei. This material is used in a companion paper (Vega et al. 2005, hereafter Paper II) to address issues such as the connection between nebular and stellar kinematics, the sensitivity of $W_{\rm CaT}$ to stellar population properties, and constraints on the contribution of a non-stellar component to the NIR spectra of AGN.

This paper is organized as follows. Section 2 describes the sample, observations and data reduction. Section 3 presents our atlas of CaT spectra, as well as [SIII]λ9069 emission line profiles for a subset of the objects. Measurements of stellar velocity dispersions are presented Section 4, while Section 5 presents results on the equivalent width of the CaT. Finally, Section 6 summarizes our main results.

2 OBSERVATIONS

The data presented here were obtained in 6 runs in 3 different telescopes: two at the 1.52m ESO-La Silla (39 galaxies), two at the KPNO 2.1m (25 galaxies), and two at the KPNO 4m telescope (16 galaxies). Although the original projects had somewhat different specific goals, they all centered on the measurement of the CaT in AGN. We have thus decided to merge all the CaT-related data in a single atlas containing the nuclear spectra and associated data-products, processed in a way as homogeneous as possible. This section describes the observations, reduction process and the general sample properties.

2.1 ESO 1.52m observations

Most of the Southern objects in the sample have been observed with the Boller & Chivens spectrograph coupled at the Cassegrain focus (f/14.9) of the now extinct 1.52m telescope, located in ESO-La Silla (Chile), during two runs (2002 March and October). Similar setups have been adopted in both runs, with a grating of 900 l/mm (# 5) centered at about 7230 Å, giving a dispersion of 1.32 Å pix^{-1} on the CCD #38 (2688×512 pixels^2, each pixel with a 15μm size). The slit width of 2″ adopted for all the program objects (which comprise the galaxies and the template stars) provided a resolution $\sigma_{\rm inst}$ of about 56 and 44 km/s for the spectra of March and October, respectively, as measured through sky emission lines. The slit was always aligned in the E-W direction (P.A. = 90°), and was long enough (4.5′) as to guarantee the inclusion of enough sky to allow its subtraction from the galaxies spectra. The plate scale on the CCD was 0.82″ pix^{-1}, and the wavelengths covered by the observations ranged from $\sim$ 6300 to 9500 Å. Wavelength calibration was performed using a HeNeArFe lamp spectra taken in each telescope position. A log of the observations is presented in Table 1. A series of velocity standard stars, listed in Table 4, have also been observed with the same setup and used as templates in the determination of $\sigma_\star$ (§4).

Since fringing effects in the NIR can be a serious concern (see below), internal flats made with a Quartz lamp have also been acquired (only in the first run) for every telescope pointing. Twilight flats have also been taken, generally at the sunset, to be used for the illumination correction. Spectrophotometric standard stars from Hamuy et al. (1994), Oke (1990), Massey et al. (1988) and Massey & Gronwal (1990) were observed (at least 2 per night), always with the slit wide open (5–8″), for flux calibration. Given the variable atmospheric conditions (particularly in the October run) our absolute flux scale is uncertain, but this has no consequence for the results reported in this paper, since we report only relative measurements.

2.2 KPNO 2.1m observations

A total of 25 Northern galaxies were observed on 2 observing runs with the KPNO 2.1m telescope, on the nights of 2002-Nov-12/13-14/15 and 2003-Feb-17/18-19/20. The observational setup was the same in both runs, resulting in spectra of similar quality to those obtained for the ESO sample. We used the Gold Camera Spectrograph with grating #35 and a slit width of 2″. The slit was oriented in the E-W direction during the first run and in the N-S direction in the second one. This configuration gives a plate scale of 0.78″ pix^{-1}, a spectral resolution of 1.24 Å pix^{-1} and a wavelength coverage of $\sim$ 6800–9300 Å. The spectral resolution for these data is $\sigma_{\rm inst} \sim 57$ km/s. A log of the observations is presented in Table 2.

The observation of each galaxy was preceded and followed by internal Quartz lamp flat-field frames (for fringing corrections) and HeNeAr wavelength calibration frames. In the case of flux and velocity standard stars, which required

Object	Activity	v_{rad} (km/s)	Morph Type	T	Date	Exp. time (s)	Flag
NGC 526A	Sy1.5	5725	S0 pec?	0.0	04 Oct 2002	(2x)1800	c
NGC 526B	Normal	5669	SB0: pec	0.0	04 Oct 2002	(1x)1500	c
NGC 1125	Sy2	3277	SB(r)0+	-1.0	30 Sep 2002	(3x)1500	c
NGC 1140	HII/Sy2	1501	IBm pec	10.0	03 Oct 2002	(3x)1500	c
NGC 1365	Sy1.8	1636	(R')SBb(s)b	3.0	02 Oct 2002	(3x)1500	d
NGC 1380	Normal	1877	SA0	0.0	30 Sep 2002	(2x)1500	c
NGC 1433	Sy2	1075	(R'$_1$)SB(rs)ab	2.0	01 Oct 2002	(3x)1500	b
NGC 1672	Sy2	1350	(R'$_1$)SB(r)bc	4.0	03 Oct 2002	(2x)1500	a
NGC 1808	Sy2	1000	(R'$_1$)SAB(s:)b	3.0	04 Oct 2002	(2x)1200	a
NGC 2997	Normal	1087	SA(s)c	5.0	11 Mar 2002	(2x)1200	a
NGC 3081	Sy2	2385	(R'$_1$)SAB(r)0	0.0	09 Mar 2002	(4x)1200	a
NGC 3115	Sy2	720	S0-	-3.0	11 Mar 2002	(1x)600	a
NGC 3256	HII	2738	Pec; merger	?	12 Mar 2002	(1x)900,(1x)1200	b
NGC 3281	Sy2	3200	SAB(rs+)a	1.0	10 Mar 2002	(4x)1200	b
NGC 3783	Sy1	2717	(R')SB(r)a	1.0	09 Mar 2002	(5x)1200	a
NGC 4507	Sy1.9	3538	SAB(s)ab	2.0	11 Mar 2002	(3x)1800	a
NGC 4593	Sy1	2698	(R)SB(rs)b	3.0	11 Mar 2002	(3x)1800	c
NGC 4748	Sy1 (NLSy1)	4386	Sa	1.0*	12 Mar 2002	(3x)1800	c
NGC 4968	Sy2	2957	(R')SAB0^0	-2.0	12 Mar 2002	(2x)1800	a
NGC 5135	Sy2	4112	SB(1)ab	2.0	11 Mar 2002	(2x)1800	a
NGC 6300	Sy2	1110	SB(rs)b	3.0	12 Mar 2002	(2x)1800	a
NGC 6814	Sy1.5	1563	SAB(rs)bc	4.0	04 Oct 2002	(3x)1500	b
NGC 6860	Sy1	4462	(R')SB(r)ab	2.0	03 Oct 2002	(3x)1500	c
NGC 6907	Normal	3161	SB(s)bc	4.0	30 Set 2002	(3x)1500	c
NGG 7130	Sy2/L	4842	Sa pec	1.0	30 Sep 2002	(3x)1500	b
NGC 7172	Sy2	2603	Sa pec sp	1.0	02 Oct 2002	(3x)1500	a
NGC 7184	Normal	2617	SB(r)c	5.0	02 Oct 2002	(3x)1500	a
NGC 7410	Sy2/L	1751	SB(s)a	1.0	04 Oct 2002	(2x)1800	a
NGC 7496	Sy2	1649	(R':)SB(rs)bc	4.0	02 Oct 2002	(3x)1500	c
NGC 7582	Sy2	1575	(R'$_1$)SB(s)ab	2.0	03 Oct 2002	(2x)1800	a
NGC 7590	Sy2	1596	S(r?)bc	4.0	30 Sep 2002	(3x)1500	a
NGC 7714	HII/L	2798	SB(s)b:pec	3.0	04 Oct 2002	(2x)1200,(1x)1500	b
IC 2560	Sy2	2925	(R':)SB(r)bc	4.0	12 Mar 2002	(3x)1800	a
IC 3639	Sy2	3275	SB(rs)bc:	4.0	10 Mar 2002	(3x)1800	a
IC 5169	Sy2	3016	(R'$_1$)SAB(r)0+	-1.0	01 Oct 2002	(3x)1500	c
ESO 362G08	Sy2	4785	Sa	1.0*	09 Mar 2002	(4x)1200	a
ESO 362G18	Sy1.5	3790	S0/a	0.0*	10 Mar 2002	(3x)1800	a
MCG-6.30.15	Sy1.2	2323	E-S0	-2.0*	10 Mar 2002	(3x)1800	a
Mrk 1210	Sy2	4046	Sa	1.0*	11 Mar 2002	(3x)1800	b

Table 1. Log of the ESO 1.52m telescope observations. Columns 2,3 and 4 list the activity type, radial velocity (in km/s) and Hubble class, all extracted from NED. Column 5 lists the numerical Hubble type, taken from RC3 (de Vaucouleurs et al. 1991), (except for those marked with asterisks, unavailable in the catalog, and whose T-types were attributed by us based on the Hubble morphological type). Column 8 lists a quality flag (see Section 3.1).

only short integrations, the fringe pattern does not vary significantly, so we obtained spectra of the Quartz and HeNeAr lamps only once, either before or after the observation of the star. During the first observing run (November) we obtained a series of twilight flats, which were used for illumination correction. However, due to bad weather conditions, we were not able to obtain twilight flats during the February run, having to resort to a combination of the program frames (excluding the regions of the spatial profiles) for the illumination correction.

Throughout the night we observed a series of velocity standard stars of various spectral types (Table 4), using the same slit width used for the observation of the galaxies. Finally, at least 3 spectrophotometric standard stars were observed every night, using a 5″ slit. We observed BD+17 4708, G191B2B and Feige 34 in the November run and Feige 66, HZ 44, Hiltner 600 and Feige 34 in the February run. As was the case in the ESO observations, not all of the KPNO observations were done under photometric conditions, however, this does not affect the outcome of this project.

2.3 KPNO 4m observations

Finally, we have incorporated to our data set the CaT observations of 14 Seyfert 2s and 2 normal galaxies taken in the KPNO 4m Mayall telescope during two runs in 1996. Table 3 describes these observations. The spectra were taken with a dispersion of 1.52 Å pix^{-1} covering the unvignetted spectral ranges 6600–9100 Å (February 1996 run) and 7400–9800 Å (October 1996 run). The slit width of 1.5″ was set at the parallactic angle. These data were partly described in

Object	Activity	v_{rad} (km/s)	Morph Type	T	Date	Exp. time (s)	Flag
Mrk 40	Sy1	6323	S0 pec	-2.0	20 Feb 2003	(4x)1200	b
Mrk 79	Sy1.2	6652	SBb	3.0	14 Nov 2002	(3x)1200	d
Mrk 372	Sy1.5	9300	S0/a	0.0*	20 Feb 2003	(3x)1200	a
Mrk 461	Sy2	4856	S0	-2.0*	19 Feb 2003	(3x)1200	b
Mrk 516	Sy1.8	8519	Sc	6.0*	15 Nov 2002	(3x)1200	b
Mrk 705	Sy1.2	8739	S0?	-2.0	15 Nov 2002	(3x)1200	c
Mrk 915	Sy1	7228	Sb	3.0*	15 Nov 2002	(3x)1200	b
Mrk 1210	Sy1/Sy2	4046	Sa	1.0*	13 Nov 2002	(3x)1200	a
Mrk 1239	Sy1.5 (NLSy1)	5974	E-S0	-3.0*	19 Feb 2003	(3x)1200	d
UGC 3478	Sy1.2	3828	Sb	3.0	20 Feb 2003	(4x)1200	d
UGC 1395	Sy1.9	5208	SA(rs)b	3.0	14 Nov 2002	(3x)1200	b
UGC 12138	Sy1.8	7487	SBa	1.0	13 Nov 2002	(3x)1200	b
UGC 12348	Sy2	7631	Sa	1.0	15 Nov 2002	(3x)1200	a
NGC 1019	Sy1	7251	SB(rs)bc	4.0	14 Nov 2002	(3x)1200	a
NGC 1142	Sy2	8648	S pec (Ring B)	1.0	14 Nov 2002	(3x)1200	c
NGC 1241	Sy2	4052	SB(rs)b	3.0	15 Nov 2002	(3x)1200	a
NGC 2639	Sy1.9	3336	(R)SA(r)a:?	1.0	13 Nov 2002	(3x)1200	a
NGC 6951	L/Sy2	1424	SAB(rs)bc	4.0	14 Nov 2002	(2x)1200	a
NGC 7469	Sy1.2	4892	(R')SAB(rs)a	1.0	13 Nov 2002	(3x)1200	a
IRAS 01475-0740	Sy2	5296	E-S0	-3.0*	13 Nov 2002	(3x)1200	c
IRAS 04502-0317	Sy2	4737	SB0/a	0.0	15 Nov 2002	(3x)1200	c
MCG -01-24-012	Sy2	5936	SAB(rs)c:	5.0	14 Nov 2002	(3x)1200	c
MCG -02-08-039	Sy2	8989	SAB(rs)a pec:	1.0	15 Nov 2002	(3x)1200	b
MCG +8-11-11	Sy1.5	6141	SB0	-2.0*	13 Nov 2002	(3x)1200	d
Akn 564	Sy1.8 (NLSy1)	7400	SB	0.0	14 Nov 2002	(3x)1200	d

Table 2. Log of the KPNO 2.1m telescope observations.

Object	Activity	v_{rad} (km/s)	Morph Type	T	Date	Exp. time (s)	Flag
Mrk 0001	Sy2	4780	S?	1.0	11 Oct 1996	(2x)1800	a
Mrk 0003	Sy2	4050	S0:	-1.0	15 Feb 1996	(2x)1800	b
Mrk 0078	Sy2	11137	SB	?	15 Feb 1996	(2x)1800	b
Mrk 0273	Sy2/L	11326	Ring Gal pec	?	15 Feb 1996	(3x)1800	c
Mrk 0348	Sy2	4507	SA(s)0/a	1.0	11 Oct 1996	(2x)1800	a
Mrk 0573	Sy2	5174	SAB(rs)0+	-1.0	11 Oct 1996	(2x)1800	a
Mrk 1066	Sy2	3605	SB(s)0+	-1.0	11 Oct 1996	(1x)1800,(1x)900	a
Mrk 1073	Sy2	6998	SB(s)b	3.0	11 Oct 1996	(1x)1800,(1x)900	a
NGC 0205	Normal	-241	dE	-5.0	15 Feb 1996	(1x)300,(2x)600	a
NGC 1068	Sy1/2	1137	SA(rs)b	3.0	11 Oct 1996	(2x)900	a
NGC 1386	Sy2	868	SB(s)0+	-1.0	11 Oct 1996	(2x)1200	a
NGC 2110	Sy2	2335	SAB0-	-3.0	15 Feb 1996	(1x)1800	a
NGC 4339	Sy2	1289	E	-5.0	15 Feb 1996	(1x)300,(2x)600	a
NGC 5929	Sy2	2492	Sab:pec	2.0	15 Feb 1996	(1x)1800,(1x)900	a
NGC 7130	Sy2/L	4842	Sa pec	1.0	11 Oct 1996	(1x)1800	b
NGC 7212	Sy2	7984	S	?	11 Oct 1996	(2x)1800	a

Table 3. Log of the KPNO 4m Mayall telescope observations.

González Delgado et al. (2001), to which we refer the reader for details of the observations and reduction process.

2.4 Reduction

Two major problems affect observations and data reductions in the NIR region: the significant contamination by atmospheric emission lines and fringing. In this section we describe how we have dealt with these problems in the reduction of the ESO and KPNO 2.1m data.

Fringing is caused by the back and forth scattering of the NIR light in coated CCDs. Here we adopted a careful procedure to eliminate fringes, or, at least, to minimize their effects. Instead of using dome-flats, we flat-fielded our data using Quartz lamp spectra, since fringes (present in all images) tend to change their locations as the telescope moves. Although for every telescope position one lamp flat was taken, in the first ESO run we decided to search for those flats which reduced the fringing patterns in the final spectrum, following the recipe given in Plait & Bohlin (1997) for

Star	Spectral Type	Telescope
HD 9737	F0III	KPNO 2.1m
HD 9748	K0III	KPNO 2.1m
HD 19136	K0III	KPNO 2.1m
HD 21910	K0III	KPNO 4m
HD 23962	K5III	KPNO 2.1m
HD 31805	F0III	KPNO 2.1m
HD 39008	K3III	KPNO 2.1m
HD 39833	G0III	KPNO 2.1m
HD 41589	K0III	KPNO 2.1m
HD 62564	K0III	KPNO 2.1m
HD 71597	K2III	KPNO 4m
HD 77189	K5III	KPNO 2.1m
HD 84059	F0III	KPNO 2.1m
HD 87018	K3III	ESO 1.52m
HD 89885	K0III	ESO 1.52m
HD 113678	K0III	ESO 1.52m
HD 116535	K0III	ESO 1.52m
HD 116565	K0III	ESO 1.52m
HD 119171	K0III	KPNO 2.1m
HD 120572	K3III	ESO 1.52m
HD 121138	K0III	ESO 1.52m
HD 121883	K0III	ESO 1.52m
HD 122665	K5III	ESO 1.52m
HD 124990	K0III	ESO 1.52m
HD 127740	F5III	KPNO 2.1m
HD 128529	K5III	ESO 1.52m
HD 132151	K0III	ESO 1.52m
HD 139447	K5III	ESO 1.52m
HD 143393	K2III	KPNO 4m
HD 143976	K5III	ESO 1.52m
HD 151817	K3III	ESO 1.52m
HD 160413	K3III	ESO 1.52m
HD 195527	K0III	KPNO 2.1m
HD 209543	K0III	KPNO 2.1m
HD 219656	K0III	KPNO 2.1m
HD 258403	F0III	KPNO 2.1m

Table 4. Velocity standard stars.

the STIS observations (where a library of fringing patterns is available for observers). In order to determine the lamp flat which minimized this effect, we performed the reduction and extraction process using each of them, for every object spectrum; the extracted spectra were then normalized in the region of interest by smoothed versions of themselves (using a 50 pixels boxcar filter), and finally an auto-correlation analysis over the normalized extracted spectrum was made. For spectra where fringing is more conspicuous, the rms in this auto-correlation function reaches higher values. By selecting the spectra whose auto-correlation function had the lowest rms in the CaT region, we automatically selected those with the smallest fringing patterns. This procedure has shown to slightly improve the final spectra, compared to no fringing correction. In any case, we have verified that these corrections have little effect upon the main data products reported in this paper, namely, stellar velocity dispersions and the CaT equivalent width.

The subtraction of atmospheric lines can introduce spurious spikes in the extracted spectra, specially near the most intense ones. This is caused by small fluctuations in the width and location of such lines along the spatial axis, so a sky region as close as possible to the extraction window is preferred. Since this often cannot be the case in observations of extended sources, we adopted a careful procedure for background removal. Possible slightly misalignments of the dispersion axis along the CCD lines were corrected applying IRAF's task *identify* to all 2D images, and a bi-dimensional function of order 6×6 was fitted through *fitcoords*. Before the fit, we analyzed carefully each object's spatial profile, to determine which CCD regions were at (or as close as possible to) the sky level; we only included in the fit the CCD regions of interest (extraction window + background), in order to achieve a better precision (residuals ≤ 0.2 Å pix^{-1}). Finally, we used the task *transform* to apply the wavelength correction to all the images before the spectral extraction. Headers from the IHAP/ESO acquisition system have been completed with the task *asthedit* from IRAF.

For both the ESO and KPNO 2.1m data we have extracted nuclear spectra adding the central 3 pixels (through the optimal extraction algorithm, Horne 1986). This corresponds to a spatial scale of $2.46''$ and $2.34''$ for the ESO and KPNO 2.1m objects, respectively.

The correction for atmospheric extinction was applied using the specific observatories data. Galactic reddening was corrected using the Cardelli, Clayton & Mathis (1989) law with $R_V = 3.1$ and the A_B values from Schlegel, Finkbeiner & Davis (1998) as listed in NED. Atmospheric telluric lines (due mainly to H_2O and O_2) have not been corrected. Nevertheless, as noticed by NW, these affect the measurement of the CaT only in galaxies with redshifts greater than about 8000 km/s, i.e., in only 4 out of 78 objects of our sample.

2.5 Sample properties

Tables 1–3 list some properties of the galaxies in the sample: including morphology, recession velocity and activity class, all extracted from the NED database. Since this list results from the merging of different observational programs, none of which aimed completeness in any sense, the resulting sample is a rather mixed bag of objects. Overall, however, this is a representative sample of Seyfert galaxies in the nearby universe.

In total, we have 80 spectra of 78 galaxies, divided into 43 Seyfert 2s, 26 Seyfert 1s (including intermediate Seyfert types and Narrow Line Seyfert 1s) and 9 non-active galaxies, including 3 Starburst nuclei. Mrk 1210 and NGC 7130 were observed twice with different telescopes. Though we keep only the better spectra in the atlas, these duplicate measurements are useful to check uncertainties in our measurements (Section 4.1). Fig 1 and Table 5 summarize some statistics of the sample, divided into Seyfert 1s, Seyfert 2s and non-active galaxies. The Far IR fluxes were compiled from NED. [OIII]λ5007 fluxes were compiled from a number of papers (Whittle 1992; Bassani et al. 1999; Schmitt et al. 2003; Storchi-Bergmann, Kinney & Challis 1995). In case of duplicate data, we favour measurements obtained under large extractions (to include more of the Narrow Line Region emission) and corrected by reddening. Inevitably, the resulting [OIII] luminosities are very inhomogeneous, and should be regarded as uncertain by a factor of ~ 2. The table shows that we span a wide range of morphological types, distances, [OIII]λ5007 and Far-IR luminosities.

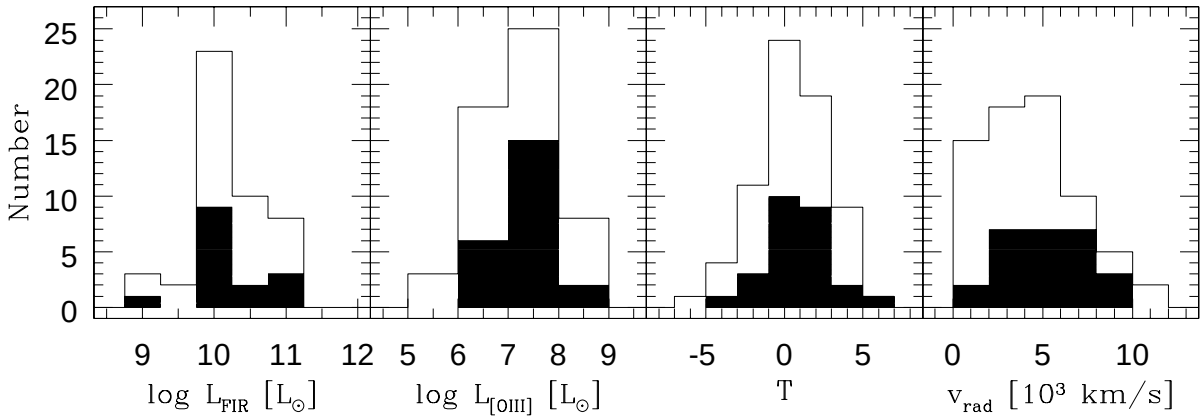

Figure 1. Sample properties. Empty areas correspond to Seyfert 2s and filled boxes to Seyfert 1s.

Summary of Sample Properties

	Seyfert 2s			Seyfert 1s			Non AGN		
	N	range	mean ± rms	N	range	mean ± rms	N	range	mean ± rms
T-type	43	(-5,5)	1.0 ± 2.3	26	(-3,6)	1.4 ± 2.1	9	(-5,10)	2.6 ± 4.2
distance [Mpc]	43	(10,151)	52 ± 36	26	(21,124)	69 ± 29	9	(1,76)	32 ± 21
r_{ap} [pc]	43	(54,715)	285±187	26	(126,734)	414±172	9	(3,459)	193±128
$\log L_{[OIII]}$ [$L_\odot$]	31	(5.6,8.7)	7.2± 0.8	23	(6.2,8.1)	7.4± 0.6			
$\log L_{FIR}$ [$L_\odot$]	31	(8.9,11.1)	10.2± 0.5	15	(9.2,11.2)	10.1± 0.5	7	(6.0,11.3)	9.6± 1.7

Table 5. Statistics of selected properties of the sample, divided into Sey 2s, Sey 1s and other galaxies. For each property we list the range, mean value and sample dispersion, and the number of objects for which the corresponding quantity was available. Luminosities were computed for $H_0 = 75$ km s^{-1}Mpc^{-1}. All properties were compiled from NED and the literature.

3 THE ATLAS

3.1 CaT spectra

Figures 2–6 present the spectra around the CaT region for all 78 galaxies in our sample. Data from different telescopes are displayed in different plots. As in NW, each panel in these figures includes an example of a velocity standard star observed through the same setup, to illustrate the kinematical broadening in the galaxy spectra. The wavelengths of the CaT lines and other features are indicated. We recall that all spectra in this atlas correspond to the nuclear regions: $2'' \times 2.46''$ for the ESO galaxies, $2'' \times 2.34''$ for the ones observed at the KPNO 2.1m and $1.5'' \times 2''$ for those observed at the KPNO 4m. Defining r_{ap} as the radius of a circle whose area equals the aperture area, our nuclear spectra corresponds to physical regions of projected radii between $r_{ap} = 50$–700 pc of the nucleus, with a median value of 286 pc (Table 5).

All spectra were brought to the rest-frame using, whenever possible, the mean redshift derived from the CaT absorption lines. For convenience, the spectra were normalized to the median flux in the 8554–8574 Å interval. We estimate the signal-to-noise ratio (S/N) by the mean/rms flux ratio in this same window. The resulting S/N spans the 8–125 range, with a median S/N of 41.

Figures 2–6 show that our NIR spectra often contain features which complicate the analysis of the CaT, such as emission lines (narrow and broad), noise and imperfectly removed atmospheric features. To help dealing with this problem we have assigned a "quality flag" to each spectrum according to the degree of contamination of the CaT lines. Column 8 of Tables 1–3 list the results. Quality *a* refers to the best spectra, where the CaT lines are little or not affected by any of the problems above, as in NGC 2997, Mrk 573 and NGC 2639 (Figures 2, 4 and 5 respectively). Quality *b* refers to reasonably good spectra, but where one of the CaT lines is contaminated. NGC 3281 (Fig 2) and Mrk 3 (Fig 4) are examples of quality *b* spectra. Quality *c* corresponds to problematic spectra, like NGC 4748 and IRAS 01475-0740 in Figs 2 and 5 respectively. CaT measurements for these objects should be treated with caution. Finally, we define as quality *d* those spectra which are so complex that it is impossible to derive any reasonably accurate CaT measurement. All such cases are presented in Fig. 6. Some Seyfert 1s and most Narrow Line Seyfert 1s in our sample fall in this category. In this latter class the CaT absorption lines are superposed to broad emission components of the same transitions from the Broad Line Region (Ferland & Persson 1989). AKN 564 and Mrk 1239 are two such cases. We have not attempted to disentangle the absorption and emission components in these cases. In some of these objects useful CaT information can be obtained from off-nuclear extractions (Paper II).

The above classification allows us to investigate how our results are affected by data quality. As expected, the S/N ratio tends to increase as one goes from quality *c* to *a*. The

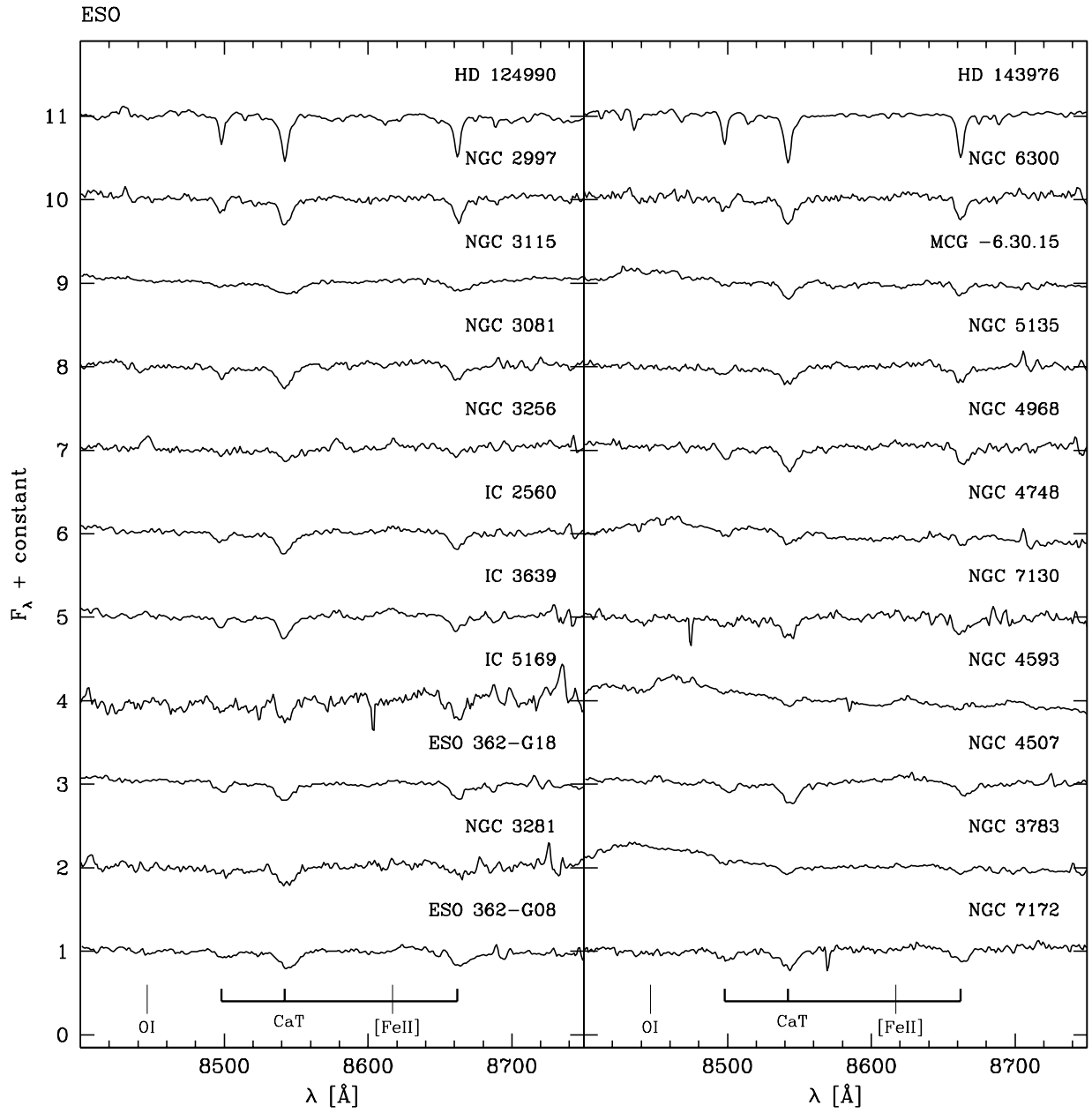

Figure 2. CaT spectra for the ESO 1.52m observations. All spectra are normalized and shifted vertically for clarity. The top spectrum in each panel corresponds to a velocity standard star observed with the same instrumental setup.

median values are $S/N = 26$, 37 and 47 for qualities *c*, *b* and *a* respectively. Also, the uncertainties in the CaT products (velocity dispersion and equivalent width) are smaller the better the quality (Sections 4 and 5).

Our data comprises 40, 15 and 17 objects with quality flags *a*, *b* and *c* respectively, totaling 72 galaxies with useful CaT spectra. This statistically significant dataset, which is similar in quality and quantity to that of NW, is analyzed in the next sections.

3.2 The [SIII]λ9069 line

In 40 galaxies the [SIII]λ9069 line is detected with at least a reasonable quality line profile (equivalent width $\gtrsim 1$ Å). The [SIII] profiles are shown in Figs 7 and 8. We have fitted this line with a single Gaussian profile. The resulting values of its width, $\sigma_{[\rm SIII]}$ (corrected for instrumental broadening) and equivalent width $W_{[\rm SIII]}$ are listed in Table 6. We do not quote [SIII] fluxes because of the uncertain absolute flux scale. The width of the [SIII] line provides a rough measure of the typical velocity of clouds in the Narrow Line Region

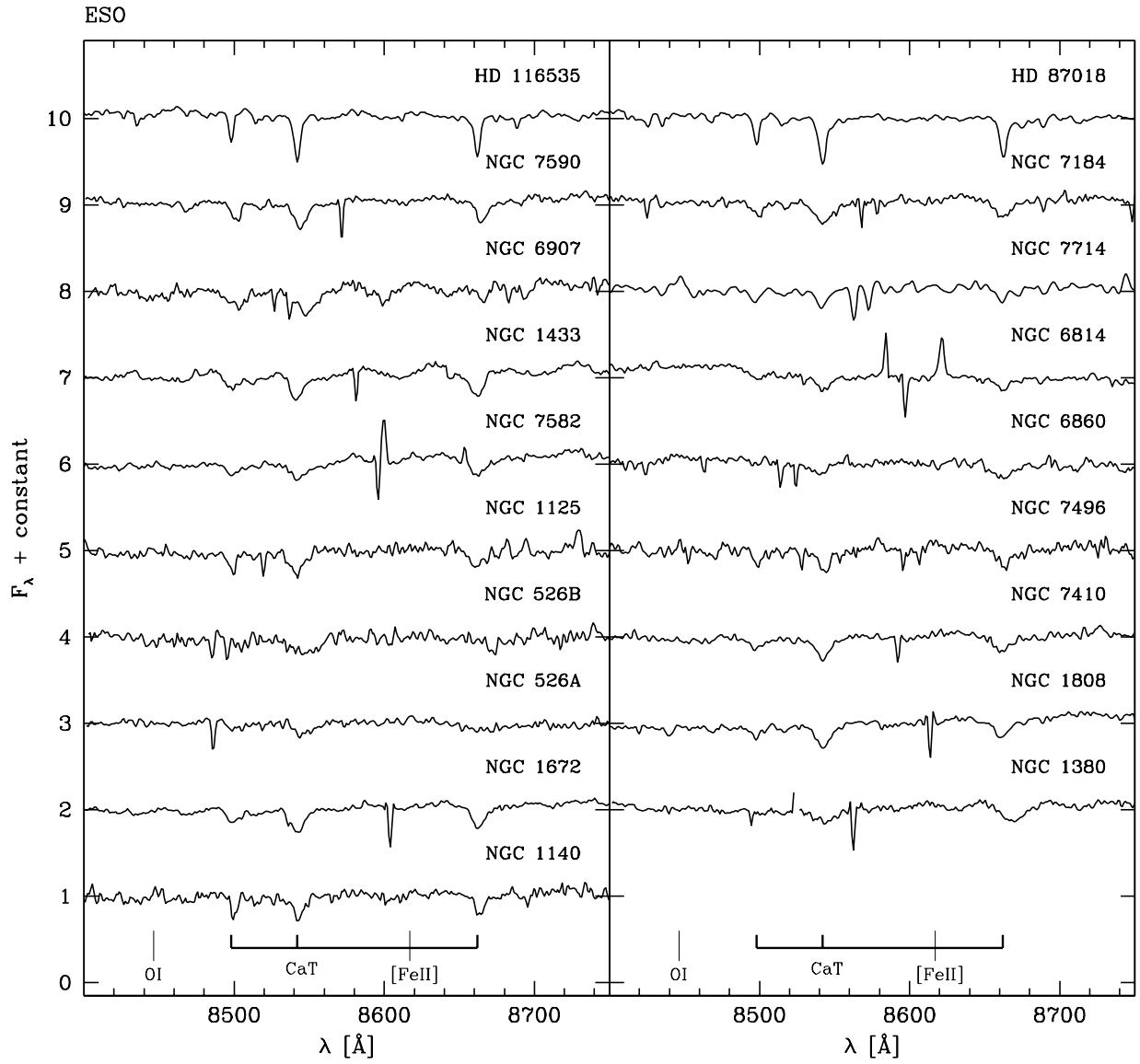

Figure 3. As Fig. 2.

(NLR) of AGN. In Paper II we compare this velocity with the typical stellar velocities deduced from the analysis of the CaT lines. Paper II also compares the $W_{[SIII]}$ values of type 1 and 2 Seyferts, which may indicate the diluting effects of an underlying AGN continuum at near-IR wavelengths.

4 STELLAR VELOCITY DISPERSIONS

Due to its location in a relatively clean spectral region, the CaT is an ideal tracer of stellar kinematics in galaxies. This potential was recognized long ago in studies of normal galaxies (Pritchet 1978; Dressler 1984) and even AGN (TDT). This is all the more true in AGN, were optical kinematical tracers like the Mg lines at ~ 5175 Å are often contaminated by emission features, which complicates the measurement of kinematical properties (NW). The combination of this practical advantage with the discovery of the $M_{\rm BH}$-$\sigma_\star$ relation brought renewed interest in the CaT as a tool to measure $\sigma_\star$, and thus indirectly weigh black holes, particularly in AGN.

In this section we present measurements of $\sigma_\star$ for galaxies in our atlas. Two different methods were employed to estimate $\sigma_\star$. In what follows we describe these methods (§4.1

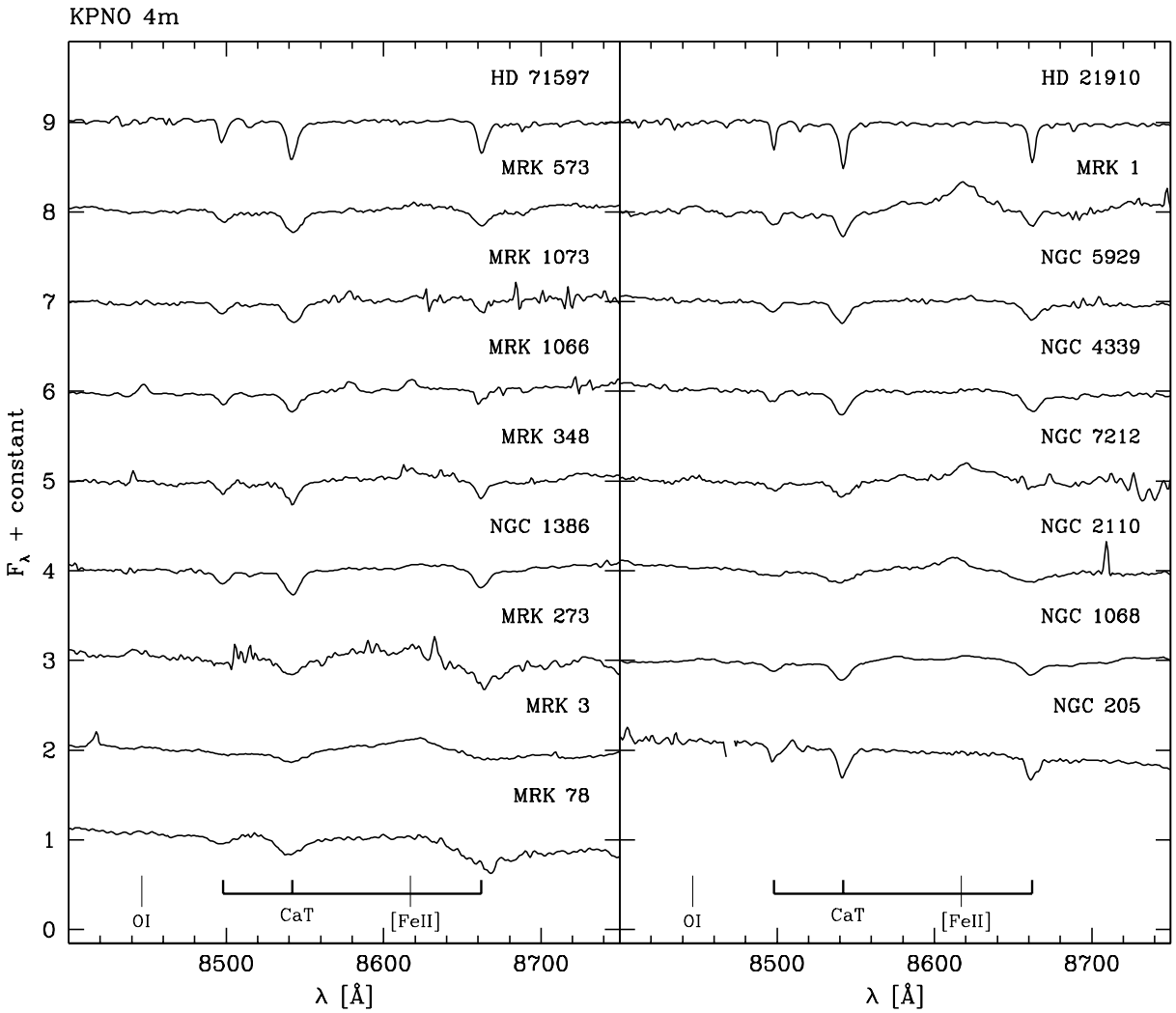

Figure 4. As Fig. 2, but for observations in the KPNO 4m telescope.

and 4.2) and compare their results both between them and with values in the literature (§4.3).

4.1 Direct Fitting Method

Kinematical parameters can be estimated by a Direct Fitting Method (DFM), which consists of fitting a model to the observed CaT spectrum directly in λ-space (Barth, Ho & Sargent 2002). A model spectrum M_λ can be built combining one or more stellar templates with a continuum C_λ, and then convolving it with an assumed Gaussian line of sight velocity distribution function $G(v_\star, \sigma_\star)$, centered at $v_\star$ and broadened by $\sigma_\star$. The resulting expression for M_λ is

$$M_\lambda = M_{\lambda_0} \left[\sum_{j=1}^{N} x_j T_{j,\lambda} r_\lambda \right] \otimes G(v_\star, \sigma_\star) \quad (1)$$

where

(i) $T_{\lambda,j}$ is the spectrum of the $j^{\rm th}$ template star normalized at λ_0. The continuum C_λ is also included in the $T_{\lambda,j}$ base as a set of power-laws with different slopes. Each galaxy was modeled with a base containing only velocity standard

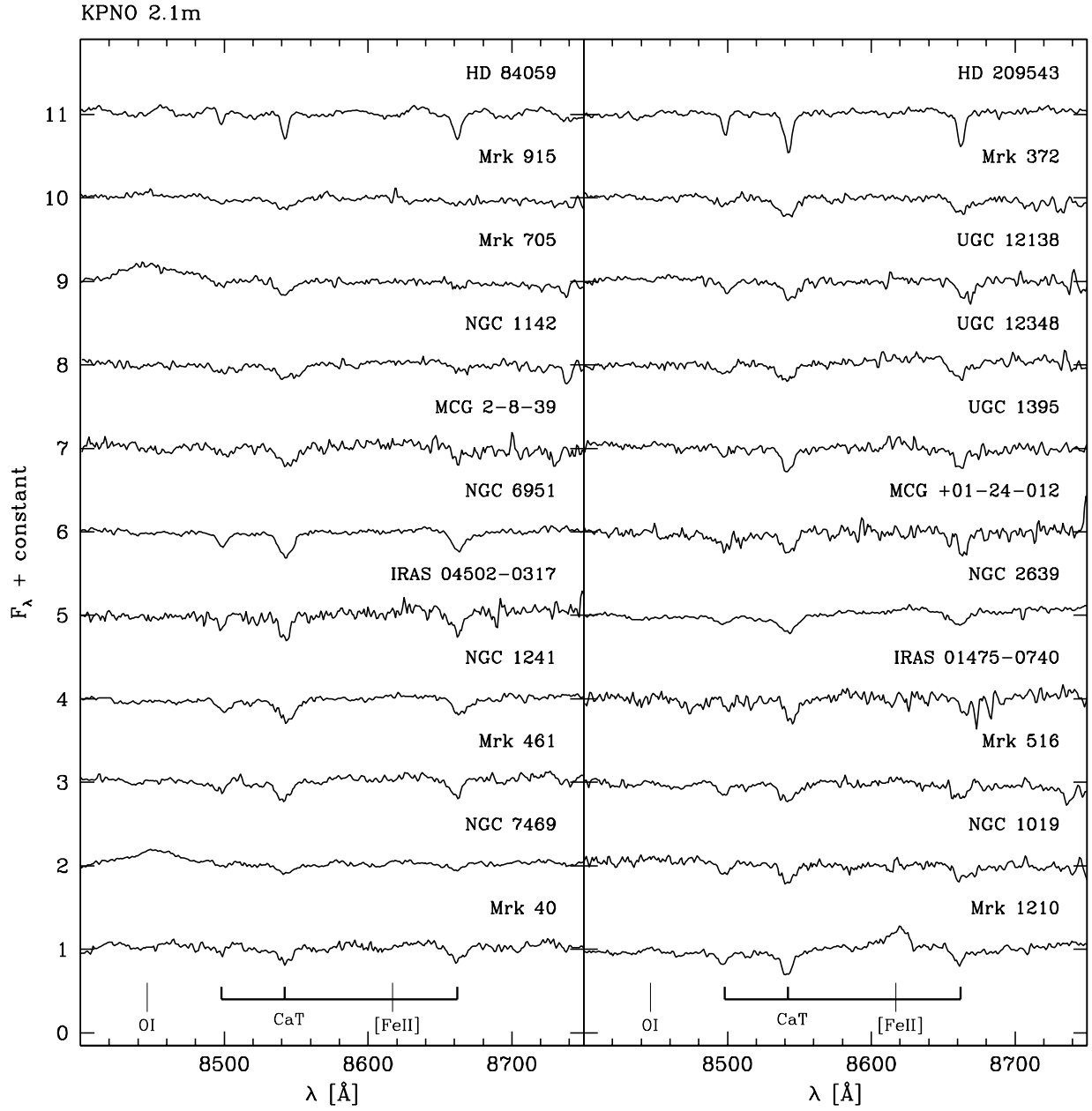

Figure 5. As Fig. 2, but for observations in the KPNO 2.1m telescope.

stars observed under the same instrumental setup, thus circumventing the need for corrections due to different spectral resolutions.
(ii) $\vec{x}$ is a vector whose components x_j $(j = 1 \ldots N)$ represent the fractional contribution of each base element to the total synthetic flux at λ_0, denoted by M_{λ_0}.
(iii) $r_\lambda \equiv 10^{-0.4(A_\lambda - A_{\lambda_0})}$ accounts for reddening by a foreground dust screen.

The continuum components in the $T_{\lambda,j}$ base are introduced with the specific aim of allowing the fits to account for a possible mismatch between the velocity standard templates and the stars in the galaxy or dilution of the CaT by an underlying continuum. It is clear that we cannot hope to constrain well the shape of C_λ given the narrow spectral range of our data. Similarly, extinction is included in the fits just for completeness, since it cannot be well constrained by the data either. Indeed, of all $N_\star+3$ parameters in the model we are only interested in one: $\sigma_\star$. The effect of $\sigma_\star$ upon M_λ is completely different from that of all the uninteresting parameters, which allows it to be well constrained by the data.

The fits are performed by minimizing the χ^2 between model and observed (O_λ) spectra:

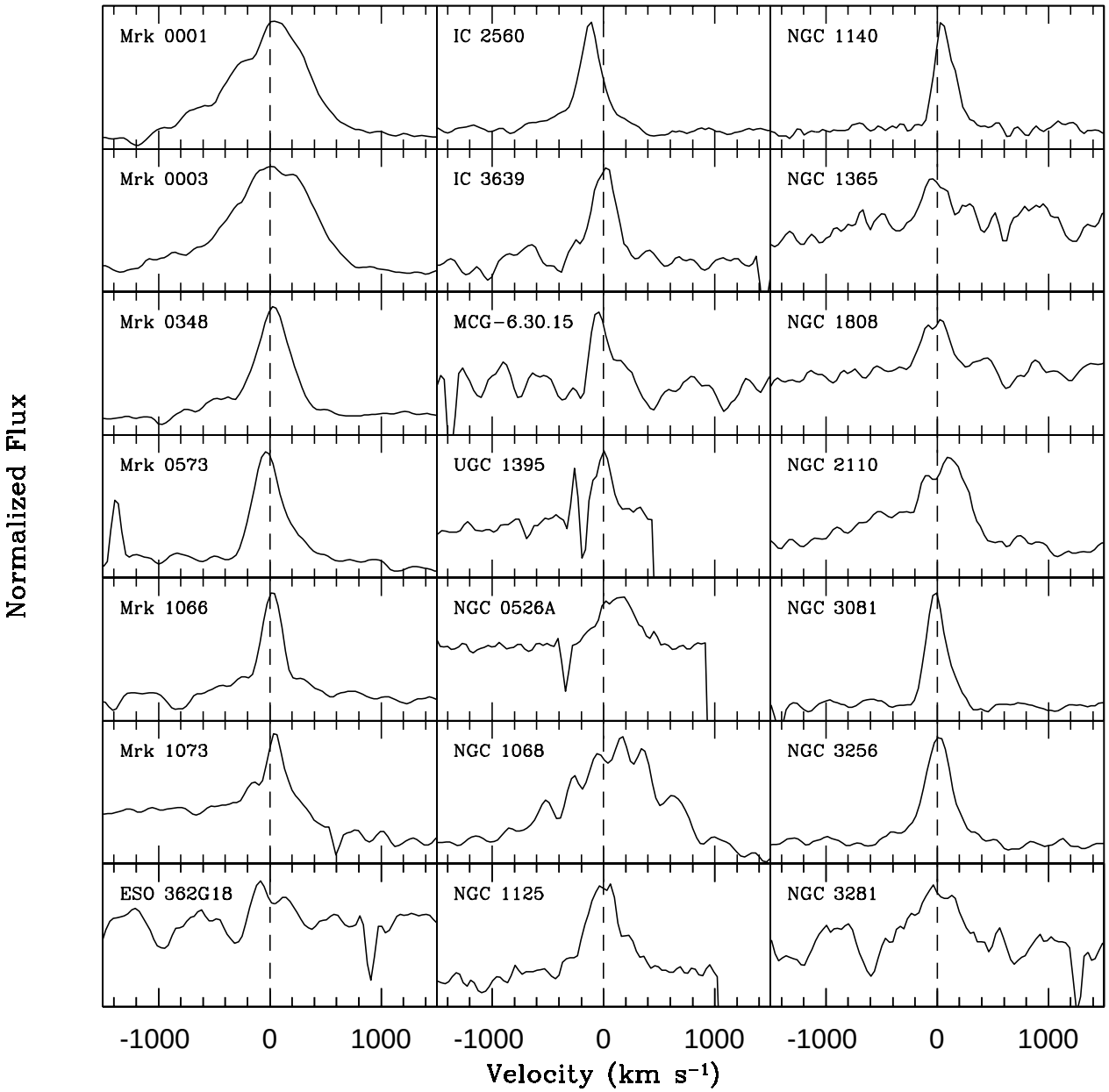

Figure 7. [SIII]λ9069 emission line profiles, normalized to the continuum level.

$$\chi^2 = \sum_{\lambda} [(O_\lambda - M_\lambda)\, w_\lambda]^2 \qquad (2)$$

where the weight spectrum w_λ is defined as the inverse of the noise in O_λ. Emission lines and spurious features, such as residual sky lines, are masked out by setting $w_\lambda = 0$. Except for the spectral base and wavelength range, this method is *identical* to the one in Cid Fernandes et al. (2004, 2005), who fit the optical spectra of galaxies by a combination of evolutionary synthesis models with the code STARLIGHT. In fact, exactly the same code was used in our fits. We thus refer the reader to those papers for details on the numerical aspects of the fits.

Figure 9 illustrates some of the resulting fits. In objects with clean CaT spectra (like NGC 1241 and NGC 2997), spectral regions outside the CaT lines were included in the fit, but we emphasize that ignoring them yields practically identical values of $\sigma_\star$. For more problematic spectra (e.g., Mrk 3 and Mrk 705), we have chosen to concentrate the fits on the CaT lines, masking out other wavelengths. The exact choice of the mask affects the derived values of $\sigma_\star$, but these

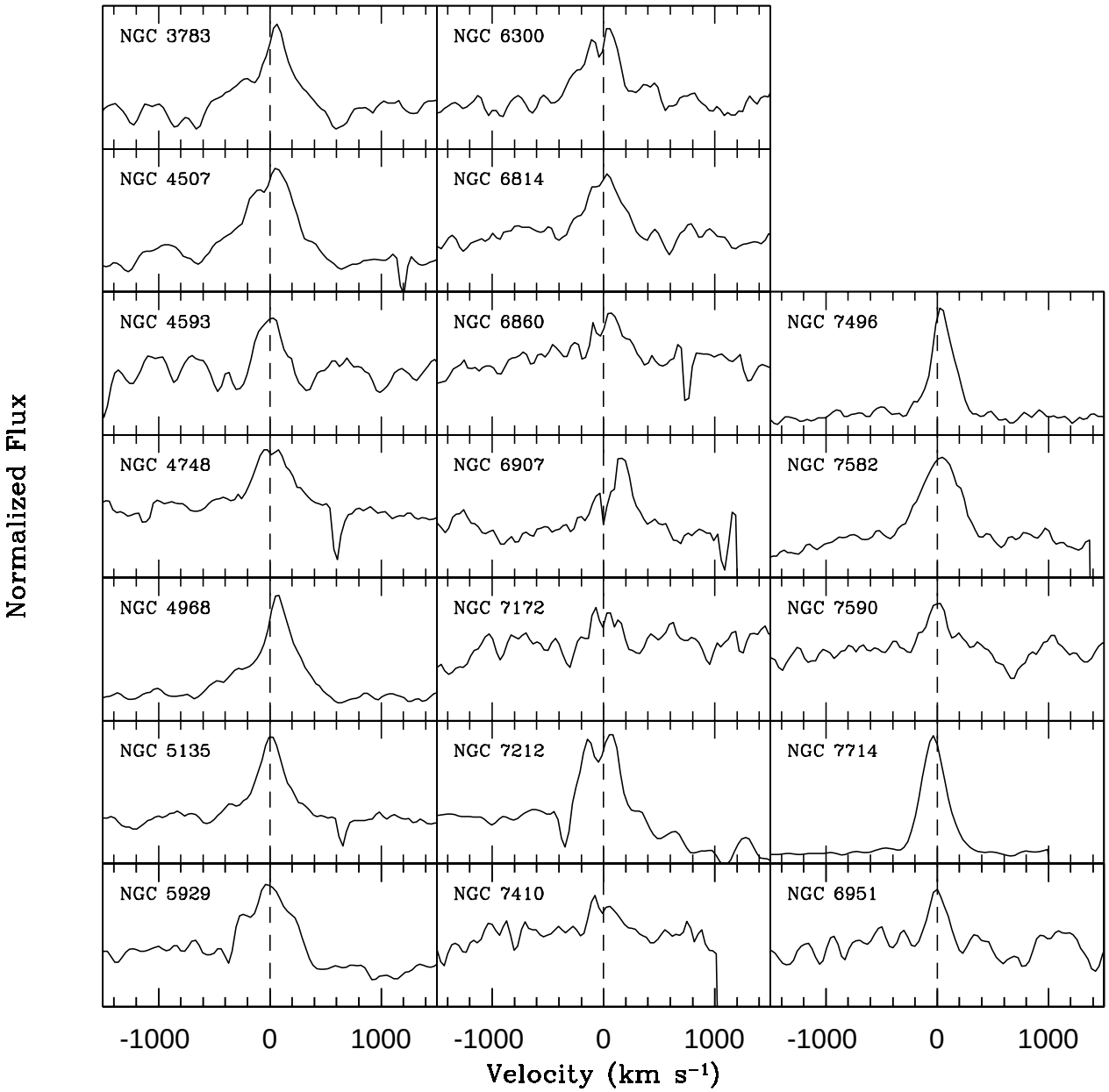

Figure 8. As Fig. 7.

variations are well within the uncertainties $\Delta\sigma_\star$ estimated below. Table 6 lists the resulting values of $\sigma_\star$.

The uncertainty in $\sigma_\star$ was estimated by the method outlined in Barth et al. (2002), which basically consists of finding the range in $\sigma_\star$ which causes an increase of $\Delta\chi^2 = 1$ over the best fit, after rescaling the errors to yield a best fit reduced χ^2 of 1. We find $\Delta\sigma_\star$ in the 3–24 km/s range (Table 6). Separating spectra according to their quality flags, we find median values of $\Delta\sigma_\star = 6$, 10 and 12 km/s for quality *a*, *b* and *c* respectively.

An independent assessment of the uncertainties is possible in the cases of Mrk 1210 and NGC 7130, for which we have repeated observations with different telescopes. For Mrk 1210, we obtain $\sigma_\star = 72\pm9$ and 77 ± 7 km/s for the ESO and KPNO 2.1 observations, respectively, while for NGC 7130 we derive $\sigma_\star = 140 \pm 8$ and 112 ± 9 km/s for the ESO and KPNO 4m data. In both cases the independent measurements are consistent to within ~ 2 sigma confidence.

A more traditional method to estimate $\Delta\sigma_\star$ consists of evaluating the dispersion among fits performed using individual template stars (e.g., Tonry & Davis 1979). For completeness, we have also evaluated $\Delta\sigma_\star$ with this method. The uncertainties obtained in this way are ~ 30 per cent larger than those obtained by the method described above.

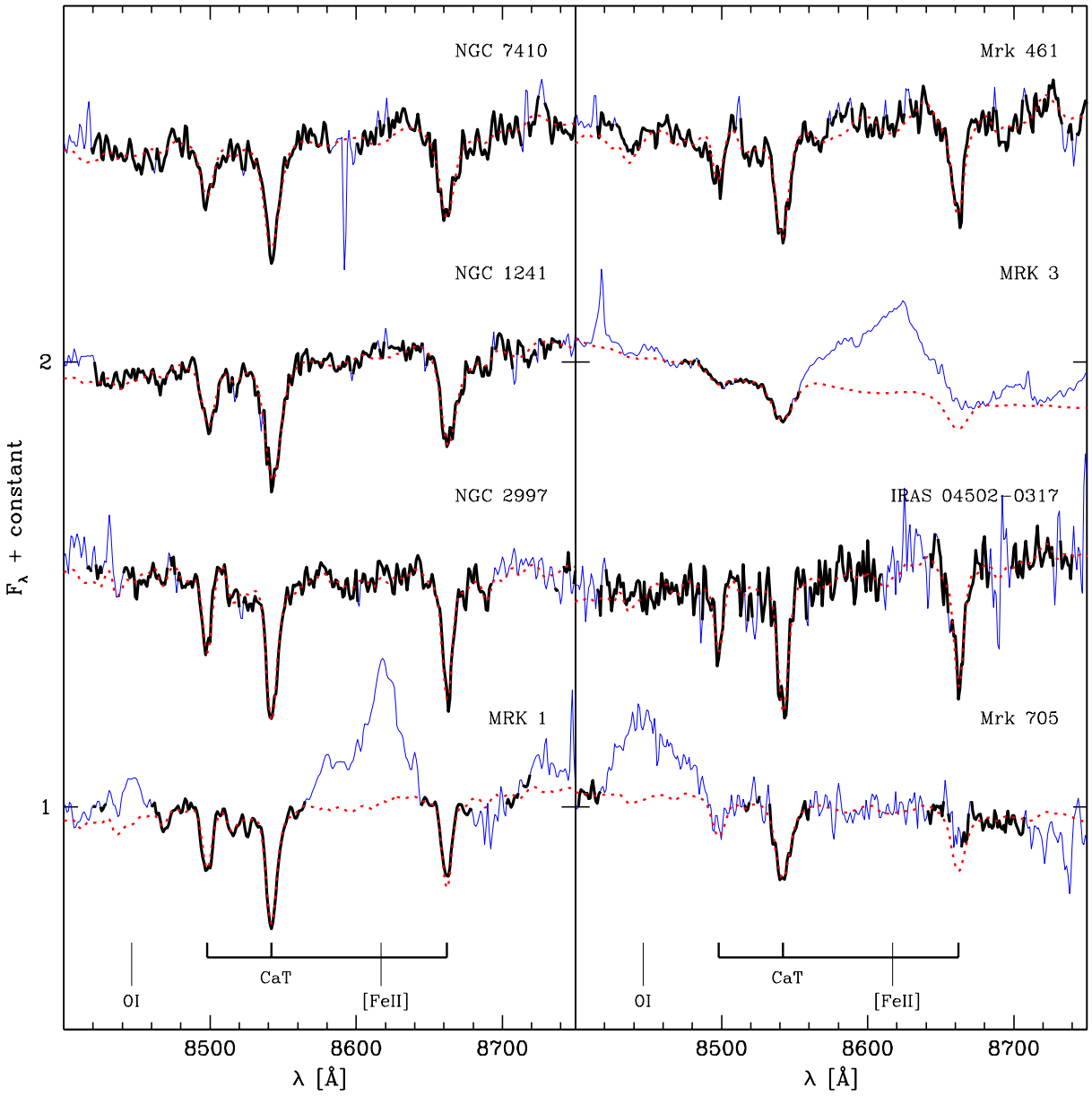

Figure 9. Examples of fits to the galaxy spectra. The solid line shows the observed spectrum, while the dotted line shows the spectral fits obtained with the DFM. A thicker line is used to mark the region actually used in the fits. NGC 7410, NGC 1241, NGC 2997 and Mrk 1 have quality flag *a*, Mrk 461 and Mrk 3 have quality *b*, IRAS 04502-0317 and Mrk 705 have quality *c*.

This agreement is hardly surprising, given that template mismatch is already accounted for in our implementation of the DFM, which includes a library of template stars in the base $T_{j,\lambda}$ (equation 1). When performing fits with a fixed $\sigma_\star$, as we do in the estimation of $\Delta\sigma_\star$ following the methodology of Barth et al. (2002), the fractions x_j associated with each template star are allowed to vary freely, which is qualitatively equivalent to changing the template star. Hence, unlike in Barth et al. (2002), there is no need to add these two estimates of $\Delta\sigma_\star$ in quadrature to obtain a total error estimate. (Doing that would increase $\Delta\sigma_\star$ by ~ 60 percent with respect to the values listed in Table 6.)

4.2 Cross-Correlation Method

One of the first techniques devised to measure velocity dispersions in galaxies is the cross-correlation method (CCM, Tonry & Davis 1979). NW review this method and show that in the CaT region it yields fairly good results. In this work, the IRAF task *fxcor* was used. In few words, *fxcor* finds the

Object	$\sigma_\star^{\rm DFM}$ (km/s)	$\sigma_\star^{\rm CCM}$ (km/s)	$\sigma_{\rm [SIII]}$ (km/s)	$W_{\rm [SIII]}$ (Å)	$W_{\rm CaT}$ (Å)
ESO 362-G08	179 ± 7	193 ± 10			7.2 ± 0.3
ESO 362-G18	126 ± 5	134 ± 4	132:	3:	6.7 ± 0.3
IC 2560	135 ± 4	138 ± 5	107	16	7.8 ± 0.4
IC 3639	95 ± 5	99 ± 5	111	10	6.3 ± 0.3
IC 5169	114 ± 12	111 ± 2			7.5 ± 0.9
IRAS 01475-0740	62 ± 11	108 ± 17			6.0 ± 0.3
IRAS 04502-0317	74 ± 8	74 ± 15			6.8 ± 0.5
MCG +01-24-012	84 ± 10	92 ± 18			6.8 ± 0.7
MCG -6.30.15	94 ± 8	103 ± 4	90	5	5.1 ± 0.5
MCG 2-8-39	170 ± 13	126 ± 11			8.0 ± 0.8
MRK 1	86 ± 4	79 ± 4	375	86	6.2 ± 0.5
MRK 3	228 ± 13	249 ± 4	364	42	4.2 ± 0.4
MRK 78	201 ± 8	186 ± 4			7.3 ± 0.3
MRK 273	211 ± 14	186 ± 2			7.7 ± 0.7
MRK 348	95 ± 6	98 ± 8	179	40	6.3 ± 0.2
MRK 573	147 ± 5	148 ± 3	171	28	7.9 ± 0.1
MRK 1066	100 ± 4	90 ± 6	119	21	5.9 ± 0.4
MRK 1073	114 ± 6	109 ± 5	168	24	5.9 ± 0.5
Mrk 40	125 ± 7	116 ± 4			4.0 ± 0.4
Mrk 372	155 ± 6	161 ± 5			6.4 ± 0.5
Mrk 461	111 ± 6	123 ± 4			5.6 ± 0.4
Mrk 516	113 ± 12	114 ± 7			7.4 ± 0.6
Mrk 705	128 ± 11	120 ± 15			5.1 ± 0.3
Mrk 915	181 ± 18	146 ± 16			5.2 ± 0.6
Mrk 1210	77 ± 7	82 ± 16			6.7 ± 0.4
NGC 205	47 ± 6	74 ± 6			6.2 ± 0.2
NGC 526A	198 ± 16	219 ± 11	159	4	4.7 ± 0.5
NGC 526B	237 ± 22	167 ± 11			7.0 ± 1.1
NGC 1019	106 ± 9	110 ± 11			6.5 ± 0.5
NGC 1068	140 ± 6	147 ± 3	543	120	6.3 ± 0.4
NGC 1125	118 ± 9	138 ± 6	168	11	7.6 ± 0.5
NGC 1140	53 ± 6	60 ± 3	81	12	5.9 ± 0.7
NGC 1142	219 ± 15	202 ± 47			8.6 ± 0.4
NGC 1241	136 ± 5	142 ± 12			8.5 ± 0.4
NGC 1380	250 ± 16	215 ± 8			7.8 ± 2.4
NGC 1386	123 ± 3	133 ± 3			8.1 ± 0.2
NGC 1433	98 ± 6	113 ± 3			7.6 ± 0.4
NGC 1672	108 ± 4	111 ± 3			7.7 ± 0.2
NGC 1808	119 ± 6	129 ± 4	129	2	7.3 ± 0.4
NGC 2110	264 ± 11	273 ± 7	375	16	6.4 ± 0.3
NGC 2639	168 ± 6	155 ± 12			7.2 ± 0.2
NGC 2997	79 ± 4	89 ± 4			8.0 ± 0.4
NGC 3081	129 ± 8	113 ± 4	77	20	7.4 ± 0.4
NGC 3115	275 ± 6	268 ± 8			7.0 ± 0.4
NGC 3256	130 ± 13	100 ± 6	120	17	3.7 ± 0.5
NGC 3281	161 ± 8	176 ± 3	235	8	7.3 ± 0.4
NGC 3783	116 ± 20	114 ± 6	247	17	3.0 ± 0.2
NGC 4339	123 ± 3	129 ± 3			7.4 ± 0.2
NGC 4507	146 ± 7	152 ± 4	229	16	7.0 ± 0.4
NGC 4593	153 ± 24	105 ± 5	96	3	3.4 ± 0.3
NGC 4748	76 ± 15	78 ± 13	187	10	3.4 ± 0.5
NGC 4968	105 ± 9	106 ± 4	182	16	6.9 ± 0.5
NGC 5135	128 ± 8	124 ± 6	135	10	6.1 ± 0.4
NGC 5929	119 ± 4	122 ± 4	195	9	6.5 ± 0.2
NGC 6300	92 ± 5	110 ± 5	217	7	8.3 ± 0.4
NGC 6814	83 ± 11	113 ± 6	169	5	4.0 ± 0.3
NGC 6860	162 ± 11	141 ± 5	153:	3:	5.6 ± 0.6
NGC 6907	157 ± 12	195 ± 15	199	6	9.2 ± 1.0
NGC 6951	115 ± 4	113 ± 12	73	2	9.0 ± 0.3

Table 6. Columns 2 and 3: Velocity dispersions obtained with the DFM and CCM methods respectively. Columns 4 and 5: Width and equivalent width of the [SIII]λ9069 emission line. Uncertain measurements are marked with a ':'. Column 6: CaT equivalent width.

Object	$\sigma_\star^{\rm DFM}$ (km/s)	$\sigma_\star^{\rm CCM}$ (km/s)	$\sigma_{\rm [SIII]}$ (km/s)	$W_{\rm [SIII]}$ (Å)	$W_{\rm CaT}$ (Å)
NGC 7130	141 ± 8	147 ± 5			6.9 ± 0.4
NGC 7172	154 ± 6	160 ± 9	112:	1:	6.9 ± 1.1
NGC 7184	146 ± 7	131 ± 5			7.9 ± 1.2
NGC 7212	143 ± 10	140 ± 2	164	26	5.3 ± 0.2
NGC 7410	144 ± 7	144 ± 6	126:	1:	7.7 ± 0.4
NGC 7469	125 ± 12	144 ± 11			2.9 ± 0.2
NGC 7496	76 ± 10	94 ± 6	96	15	5.8 ± 0.7
NGC 7582	121 ± 7	113 ± 3	180	8	5.9 ± 0.5
NGC 7590	93 ± 4	90 ± 4	136	2	7.7 ± 2.0
NGC 7714	59 ± 9	65 ± 4	105	28	4.7 ± 2.4
UGC 1395	66 ± 6	62 ± 16	47:	4:	6.5 ± 0.4
UGC 12138	115 ± 10	136 ± 8			6.9 ± 0.6
UGC 12348	155 ± 9	165 ± 14			7.6 ± 0.4

Table 7. Continuation of Table 6.

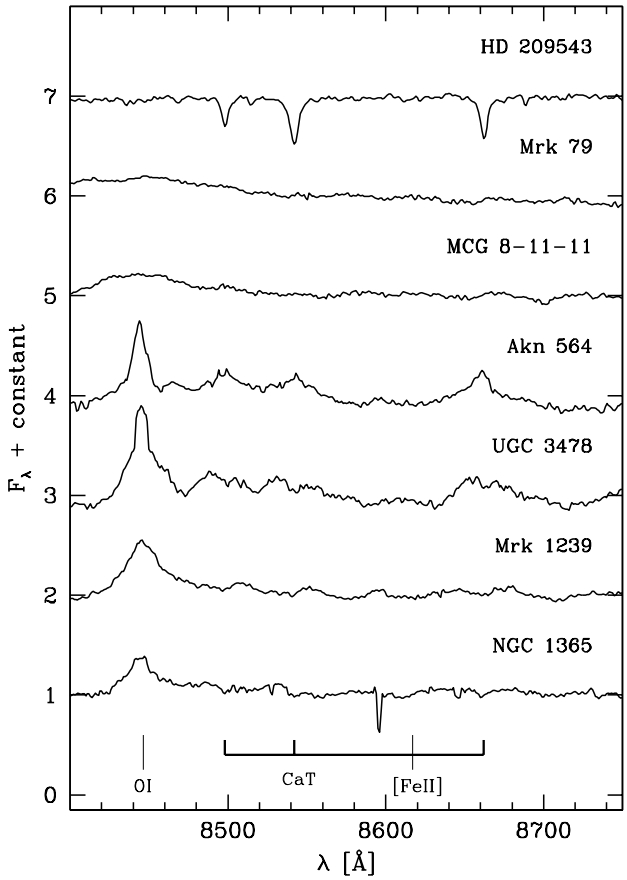

Figure 6. Objects containing complex (quality flag = *d*) spectra in the CaT region.

cross-correlation function between the galaxy and the template spectra in Fourier space. The peak of this function is then modeled by a Gaussian. We use the same individual masks which were used in the DFM, and we allow a linear continuum subtraction from the galaxy spectra. The output from *fxcor* is calibrated in order to account for instrumental resolution. Column 3 of Table 6 presents $\sigma_\star$ values obtained with this method. Uncertainties in this case are evaluated from the rms in $\sigma_\star$ values obtained using different template stars.

We find that the DFM and the CCM yield velocity dispersions consistent to within 19 km/s on-average. The agreement is much better for quality *a* spectra, for which the difference between $\sigma_\star^{\rm DFM}$ and $\sigma_\star^{\rm CCM}$ is just 9 km/s in the rms. For quality *b* and *c* the DFM and CCM methods agree to rms dispersions of 20 and 30 km/s respectively, which further confirms that data quality is the major source of uncertainty in $\sigma_\star$. The uncertainties $\Delta\sigma_\star$ obtained with these two methods are also similar, with an rms difference of 6 km/s.

4.3 Comparison with previous results

In Fig. 10 we compare our DFM measurements of $\sigma_\star$ with values compiled from the literature for objects in common. The two major sources of $\sigma_\star$ are NW and Cid Fernandes et al. (2004), which have 14 and 22 objects in common with our sample, respectively. NW derive $\sigma_\star$ from the cross-correlation method applied to either the CaT or the Mg lines in the optical, while Cid Fernandes et al. (2004) estimate $\sigma_\star$ fitting the 3500–5200 Å spectra of Seyfert 2s with a combination of single stellar populations from the Bruzual & Charlot (2003, hereafter BC03) models. These two studies agree in their estimates of $\sigma_\star$ at the level of ±21 km/s rms.

Our CaT-based estimates of $\sigma_\star$ are in good agreement with these previous estimates. The rms difference between our values and those in the literature is 22 km/s. The spread is somewhat smaller for quality *a* data (rms of 21 km/s) than for qualities *b* and *c* (25 km/s). Furthermore, on average, our estimates of $\sigma_\star$ are just 4 km/s lower than those in the literature. Very similar results are obtained comparing our CCM-based estimates of $\sigma_\star$ with literature data, which also yields an rms of 22 km/s. Given the differences in data qual-

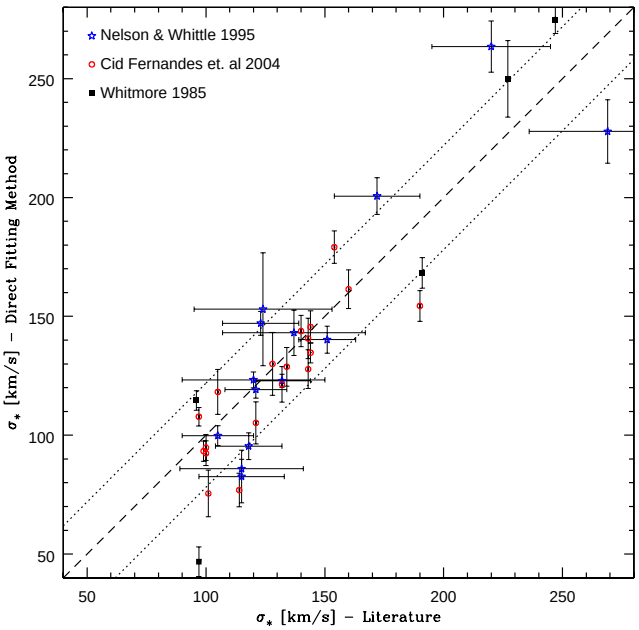

Figure 10. Comparison of the stellar velocity dispersions estimated in this work and values compiled from the literature. The identity line is traced by the dashed line, while dotted lines indicate the ±22 km/s global dispersion (= 1 sigma).

ity, spatial extractions, method of analysis, and the intrinsic uncertainties in $\sigma_\star$, we conclude that there are no significant differences between our estimates of $\sigma_\star$ and those reported in previous studies. In any case, the level of agreement is very similar to those among other studies.

We also made a compilation from Oliva et al. (1995, 1999) near-IR CO and Si $\sigma_\star$ estimates, where we can find 9 objects in common with our sample. Although the two estimates are very likely to be correlated ($P_{rs} \approx 2.5\%$), here the difference between results is higher than when compared with optical data, indicating that our estimated $\sigma_\star$ is, on average, lower by 34 km/s. Considering just the 6 objects that have an "a" fitting quality, this difference practically does not change (33 km/s), having a rms of 38 km/s (i.e., agrees with our results within a 0.05 confidence level, considering that their errors are also of 20 km/s).

5 EQUIVALENT WIDTHS

Besides its use as a tracer of stellar kinematics, the CaT provides information on the properties of stellar populations in galaxies. The most extensive and up-to-date study of the CaT in stars and as a diagnostic of stellar populations in galaxies has been published by Cenarro and co-workers in the last few years (Cenarro et al. 2001a, 2001b, 2002, 2003; Vazdekis et al. 2003). As summarized in the introduction (see also Paper II), recent work reveals serious difficulties in interpreting the observed strength of the CaT in normal galaxies, which in turn raises doubts as to the usefulness of the CaT as a stellar population diagnostic. Clearly, the situation in AGN ought to be even more problematic than for normal galaxies, given: (1) the presence of emission lines around the CaT, (2) the fact that many AGN are known to be surrounded by starbursts of various ages and intensities, and (3) the presence of an underlying non-stellar continuum, seen either directly (in Seyfert 1s) or scattered (Seyfert 2s).

Notwithstanding these caveats, in this section we present measurements of the CaT equivalent width for objects in our sample. These data is used in Paper II to evaluate the presence of an AGN continuum at NIR wavelengths, and to investigate how our AGN fit into the CaT-$\sigma_\star$ relation (e.g., Michielsen et al. 2003).

We measure the CaT strength following Cenarro et al. (2001a), who offer two definitions of the CaT equivalent width: 'CaT' (which we call $W_{\rm CaT}$), which consists of a sum of the equivalent widths of all three CaT lines, and 'CaT*' (called $W_{\rm CaT*}$ here), which corrects $W_{\rm CaT}$ for contamination by Paschen line absorption. These equivalent widths are measured with respect to a continuum defined by fitting the spectrum in 5 windows in the 8474–8792 Å range.

It is evident from Figs. 2–5 that this recipe cannot be blindly applied to our spectra, given the presence of emission lines, atmospheric and noise artifacts which affect both the continuum, CaT and Paschen bandpasses. On the other hand, in Section 4.1 we have seen that the DFM provides good matches to the clean regions of the spectra. Naturally, these model spectra do not suffer from the aforementioned problems. Measuring the CaT indices over the model fits is therefore a simpler alternative to removing the unwanted features from the observed spectra. (A similar strategy was employed by Cid Fernandes et al. 2004 in their analysis of optical spectra of Seyfert 2s.) We thus opted to measure both $W_{\rm CaT}$ and $W_{\rm CaT*}$ over the synthetic spectra.

We tested the validity of this procedure by comparing the values of $W_{\rm CaT}$ measured for the model (M_λ) and observed (O_λ) spectra for galaxies with no serious contamination, or galaxies where the spurious features can be easily removed (say, by chopping narrow emission lines). We find that these two estimates of $W_{\rm CaT}$ agree well, with an rms difference of 0.4 Å. There is a small bias, in the sense that $W_{\rm CaT}$ values measured over the synthetic spectra are on average 0.5 Å smaller than those measured over the observed spectrum, generally due to noise in the redder continuum band. Both this offset and the rms difference are comparable to the formal uncertainties in $W_{\rm CaT}$. We thus conclude that this experiment validates our strategy of measuring $W_{\rm CaT}$ over the model spectra.

Although Cenarro et al. (2001a) and subsequent studies of normal galaxies favour $W_{\rm CaT*}$ over $W_{\rm CaT}$ as a measure of the CaT strength, we have reasons to do the opposite choice. Firstly, in several cases our DFM fits concentrate on windows centered nearly exclusively on the CaT lines. Hence, Paschen lines, even if present in the spectrum (which is not the case in any of our spectra, with the possible exception of the normal galaxy NGC 6907), would not have a relevant weight in the spectral fits. Secondly, only the KPNO 2.1m observations include velocity standard stars with Paschen absorption lines in their spectra (F giants; see Table 4). For the other runs, the spectral base $T_{j,\lambda}$ does not cover such spectral types, so the synthetic spectrum cannot possibly model any Paschen line absorption properly, thus rendering the Paschen line correction in $W_{\rm CaT*}$ meaningless. Hence, we only present $W_{\rm CaT}$ measurements (Table 6).

Since the M_λ spectra are effectively noiseless, in order

to compute uncertainties in $W_{\rm CaT}$ we carried out a formal propagation using the S/N derived for each galaxy (Section 3.1). To be on the conservative side, we further add 0.5 Å in quadrature to account for the empirically established rms difference between $W_{\rm CaT}$ measurements performed over M_λ and over clean O_λ spectra. The median uncertainties are $\Delta W_{\rm CaT} = 0.6$, 0.7 and 0.8 Å for quality *a*, *b* and *c* spectra respectively.

Inspection of the $W_{\rm CaT}$ values in Table 6 shows that this index spans a range of values from $\sim$ 1 to 9 Å. However, most values are within the 6–8 Å range, giving the false impression that stellar populations are very homogeneous in our sample. This is definitely not true, as we know from independent work at other wavelengths for many of the same galaxies studied here (e.g., Cid Fernandes et al. 2001, 2004). Instead, the small variation in CaT strength reinforces the notion that this feature is not much sensitive to stellar population properties. The only noticeable trend is that Seyfert 1s tend to have weaker CaT than other galaxies. On the mean, $W_{\rm CaT} = 4.6 \pm 2.0$ Å (sample dispersion) for Seyfert 1s and 7.0 ± 1.0 Å for Seyfert 2s. The statistics for the 3 starbursts in our sample is 4.7 ± 1.1 Å, while for the remaining 6 non-active galaxies $W_{\rm CaT} = 7.7 \pm 1.0$ Å, very similar to the values spanned by Seyfert 2s. The most likely origin for the difference between type 1 and type 2 AGN is dilution by an underlying non-stellar featureless continuum in type 1s. Hence, if on the one hand $W_{\rm CaT}$ turns out to be a rather poor tracer of stellar populations, it seems to be a good FC detector. These aspects are explored in greater depth in Paper II.

6 CONCLUSIONS

This paper presented a spectroscopic atlas of 78 galaxies in the region around the Calcium triplet (CaT). Most of the objects are AGN, split into 43 type 2 Seyferts and 26 type 1s. The spectra cover the inner $r_{pc} \sim 300$ pc with a typical S/N of 40. Quality flags were assigned to each spectrum to describe the degree of contamination of the CaT absorption lines by emission lines or atmospheric features. The main products from our analysis of this data set are stellar velocity dispersions, [SIII]λ9069 line profiles, and CaT equivalent widths.

Stellar velocity dispersions ($\sigma_\star$) were measured for 72 of the spectra using both direct fitting and cross-correlation methods. The two techniques yield results compatible to within an rms of 19 km/s, which is also the typical uncertainty of our estimates. Comparison with $\sigma_\star$ values reported in the literature for objects in common agree with our estimates at the level of $\sim$ 20 km/s rms for optical data, and at a 2 sigma level for near-IR data.

We have also analyzed the [SIII]λ9069 line profiles for 40 galaxies in the sample with useful data in this range. Single Gaussian fits were performed, producing estimates of line width and equivalent width.

The CaT equivalent width was measured over the synthetic spectra obtained from the direct fits, circumventing the manual editing of the spectra which would be required to remove undesirable features which affect $W_{\rm CaT}$. We find that the value of $W_{\rm CaT}$ in Seyfert 2s and normal galaxies are concentrated in a relatively small range, from $\sim$ 6 to 8 Å. Type 1 Seyferts tend to have a weaker CaT, most likely due to dilution by a non-stellar continuum.

These data products are analyzed in Paper II, where we investigate the relation between nebular and stellar kinematics and the behaviour of the CaT strength as a function of activity type and stellar population properties.

ACKNOWLEDGMENTS

AGR, LRV, NVA, RCF and TSB acknowledge the support from CAPES, CNPq and Instituto do Milênio. RGD acknowledges support by Spanish Ministry of Science and Technology (MCYT) through grant AYA-2004-02703. AGR and LRV aknowledge A. Rodríguez-Ardila for suggestions in the reduction process. We thank the Laboratório Nacional de Astrofísica for the allocation of time on the ESO 1.52m and financial support during the runs. Part of the data described here were taken at Kitt Peak National Observatory, National Optical Astronomy Observatories, which are operated by AURA, Inc., under a cooperative agreement with the National Science Foundation. Basic research at the US Naval Research Laboratory is supported by the Office of Naval Research. This research made use of the NASA/IPAC Extragalactic Database (NED), which is operated by the Jet Propulsion Laboratory, Caltech, under contract with NASA.

REFERENCES

Barth A.J., Ho L.C., Sargent W.L.W., 2002, ApJ, 566, L13.
Barth A.J., Ho L.C., Sargent W.L.W., 2003, ApJ, 583, 134.
Barth A.J., Ho L.C., Rutledge R.E., Sargent W.L.W., 2004, ApJ, 607, 90.
Barth A.J., Greene J.E., Ho L.C., 2005, ApJL, in press (astro-ph/0412575).
Bassani L., Dadina M., Maiolino R., Salvati M., Risaliti G., Della Ceca R., Matt G., Zamorani G., 1999, ApJS, 121, 473.
Botte V., Ciroi S., di Mille F., Rafanelli P., Romano A., 2004, MNRAS, 356, 789.
Bruzual G., Charlot S., 2003, MNRAS, 344, 1000.
Cardelli J.A., Clayton G.C., Mathis J.S., 1989, ApJ, 345, 245.
Cenarro A.J., Cardiel N., Gorgas J., Peletier R.F., Vazdekis A., Prada F., 2001a, MNRAS, 326, 959.
Cenarro A.J., Gorgas J., Cardiel N., Pedraz S., Peletier R.F., Vazdekis A., 2001b, MNRAS, 326, 981.
Cenarro A.J., Gorgas J., Cardiel N., Vazdekis A., Peletier R.F., 2002, MNRAS, 329, 863.
Cenarro A.J., Gorgas J., Vazdekis A., Cardiel N., Peletier R.F., 2003, MNRAS, 339, 12.
Cenarro A.J., Sánchez-Blázquez P., Cardiel N., Gorgas J., 2004, ApJ, 614, 101.
Cid Fernandes R., Terlevich R.J., 1995, MNRAS, 272, 423
Cid Fernandes R., Heckman T., Schmitt H., González Delgado R.M., Storchi-Bergmann T., 2001, ApJ, 558, 81.
Cid Fernandes R., Gu Q., Melnick J., Terlevich E., Terlevich R., Kunth D., Rodrigues Lacerda R., Joguet B., 2004, MNRAS, 355, 273.
Cid Fernandes R., Mateus A., Sodré L., Stasinska G., Gomes J.M., 2005, MNRAS, in press (astro-ph/0412481).
Dressler A., 1984, ApJ, 286, 97.
Falcón-Barroso J., Peletier R.F., Vazdekis A., Balcells M., 2003, ApJ, 588, 17.
Ferland G.J., Persson S.E., 1989, ApJ, 347, 656.
Ferrarese L., Merritt D., 2000, ApJ, 539, 9.

Ferrarese, L., Pogge, R. W., Peterson, B. M., & Merritt, D. 2001, ApJ, 555, L79
Filippenko A.V., Ho L.C., 2003, ApJ, 588, L13.
Gebhardt K., Bender R., Bower G., Dressler A., Faber S.M., et al., 2000, ApJ, 539, 13.
González Delgado R., Heckman T., Leitherer C., 2001, ApJ, 546, 845.
Hamuy M., Suntzeff N.B., Heathcote S.R., Walker A.R., Gigoux P., Phillips M.M., 1994, PASP, 106, 566.
Heckman T., Krolik J., Meurer G., Calzetti D., Kinney A., Koratkar A., Leitherer C., Robert C., Wilson A., 1995, ApJ, 452, 549.
Heckman T., Gonzalez Delgado R., Leitherer C., Meurer G., Krolik J., Wilson A.S., Koratkar A., Kinney A., 1997, ApJ, 482, 114.
Horne K., 1986, PASP, 98, 609.
Jiménez-Benito L., Díaz A.I., Terlevich R.J., Terlevich E., 2000, MNRAS, 317, 907.
Massey P., Strobel K., Barnes J.V., Anderson E., 1988, ApJ, 328, 315.
Massey P., Gronwall C., 1990, ApJ, 358, 344.
Michielsen D., De Rijcke S., Dejonghe H., Zeilinger W.W., Hau G.K.T., 2003, ApJ, 597, 21.
Nelson C.H., Whittle M., 1995, ApJS, 99, 67.
Nelson C.H., Whittle M., 1996, ApJ, 465, 96.
Nelson C.H., Green R.F., Bower G., Gebhardt K., Weistrop D., 2004, ApJ, 615, 652.
Oke J.B., 1990, AJ, 99, 1621.
Oliva E., Origlia L., Kotilainen J.K., Moorwood A.F.M., 1995, A&A, 301, 55..
Oliva E., Origlia L., Maiolino R., Moorwood A.F.M., 1999, A&A, 350, 90.
Onken C.A., Ferrarese L., Merritt D., Peterson B.M., Pogge R.W., Vestergaard M., Wandel A., 2004, ApJ, 615, 645.
Plait P., Bohlin R., 1997, *Fringe Science: Creating a STIS CCD Fringe Flat Field*, In: The 1997 HST Calibration Workshop, eds. Casertano S., et al., STScI.
Pritchet C., 1978, ApJ, 221, 507.
Saglia R.P., Maraston C., Thomas D., Bender R., Colless M., 2002, ApJ, 579, 13.
Schlegel D., Finkbeiner D., Davis M., 1998, ApJ, 500, 525.
Schmitt H., Donley J.L., Antonucci R.R.J., Hutchings J.B., Kinney A.L., 2003, ApJS, 148, 327.
Storchi-Bergmann T., Kinney A.L., Challis P., 1995, ApJS, 98, 103.
Terlevich E., Díaz A.I., Terlevich R.J., 1990, MNRAS, 242, 271
Thomas D., Maraston C., Bender R., 2003, MNRAS, 343, 279.
Tonry J., Davis M., 1979, AJ, 84, 1511.
Tremaine S., Gebhardt K., Bender R., Bower G., Dressler A., et al., 2002, ApJ, 574, 740.
de Vaucouleurs G., de Vaucouleurs A., Corwin H.G.Jr., Buta R.J., Paturel G., Fouque P., 1991, *Third Reference Catalog of Bright Galaxies*, v.1-3, Springer-Verlag Berlin Heidelberg New York.
Vazdekis A., Cenarro A.J., Gorgas J., Cardiel N., Peletier R.F., 2003, MNRAS, 340, 1317.
Vega L.R., Asari N.V., Cid Fernandes R., Garcia-Rissmann A., Schmitt H., González Delgado R.M., Storchi-Bergmann T., 2005, in preparation.
Whitmore B.C., McElroy D.B., Tonry J.L., 1985, ApJS, 59, 1.
Whittle M., 1992, ApJS, 79, 49.